การทำนายอัตราการถ่ายเทความร้อนในเงื่อนไขสถานะชั่วครู่ของเครื่องแลกเปลี่ยนความร้อนชนิดท่อความร้อนโดยใช้แบบจำลองสามมิติ

Prediction of Heat Transfer Rate under Transient Condition in Heat Pipe Heat Exchanger Using Three-dimensional Model

สุพัตรา บุไธสง[1*] สัมพันธ์ ฤทธิเดช[2] ธีรพัฒน์ ชมภูคำ[3] มนตรี ทองมูล[4] และ Yulong Ding[5]

[1]นักศึกษา [2]รองศาสตราจารย์ [3]ผู้ช่วยศาสตราจารย์ สาขาวิศวกรรมเครื่องกล คณะวิศวกรรมศาสตร์ มหาวิทยาลัยมหาสารคาม จังหวัดมหาสารคาม 44150

[4]อาจารย์ ภาควิชาคณิตศาสตร์ คณะวิทยาศาสตร์ มหาวิทยาลัยมหาสารคาม จังหวัดมหาสารคาม 44150

[5]Professor, School of Chemical Engineering, The University of Birmingham B15 2TT, United Kingdom

บทคัดย่อ

การศึกษาครั้งนี้มีวัตถุประสงค์พัฒนาแบบจำลองสามมิติที่สภาวะชั่วครู่เพื่อใช้ทำนายอัตราการถ่ายเทความร้อนของเครื่องแลกเปลี่ยนความร้อนชนิดท่อความร้อน และเปรียบเทียบผลที่ได้จากการแบบจำลองกับผลการทดลอง ซึ่งงานวิจัยนี้ได้นำเสนอรายละเอียดในการคำนวณแต่ละส่วนของท่อความร้อนซึ่งประกอบด้วย ผนัง วัสดุพรุน และแนวแกนไอ โดยประมวลผลเชิงตัวเลขด้วยระเบียบวิธีไฟไนต์เอเลเมนต์ จากการประมวลผลแบบจำลองจะได้ค่าอัตราการถ่ายเทความร้อนของท่อความร้อนเพื่อนำไปออกแบบเครื่องแลกเปลี่ยนความร้อนชนิดท่อความร้อน ซึ่งจาก การประมวลผลและการทดลองพบว่าเปอร์เซ็นต์ที่ได้จากแบบจำลองเปรียบเทียบกับผลการทดลองโดยใช้สารทำงาน น้ำกลั่น, เอทานอล และ R134a เท่ากับ 10.3%, 10.4% และ 6.7% ตามลำดับ และได้ค่าอัตราการถ่ายเทความร้อนจากการทดลองโดยใช้สารทำงานน้ำกลั่น, เอทานอล และ R134a เท่ากับ 627.3 วัตต์, 522.8 วัตต์ และ 836.4 วัตต์ ตามลำดับ

Abstract

The aim of this study was to develop a three-dimensional transient condition model to predict the heat transfer rate of a heat pipe heat exchanger. This paper presents the details of the calculated domains, which consist of the wall, wick, and vapor core. They were numerically simulated using the finite element method. The heat transfer rate values obtained from the model simulation can be used to design heat pipe heat exchangers. The values obtained from the model calculation were then compared with the results from experiments, and the differences were 10.3%, 10.4%, and 6.7% for the working fluids of distilled water, ethanol, and R134a, respectively. The working fluids of distilled water, ethanol, and R134a obtained heat transfer rates of 627.3 watts, 522.8 watts, and 836.4 watts from the experiments, respectively.

คำสำคัญ : อัตราการถ่ายเทความร้อน เงื่อนไขสถานะชั่วครู่ เครื่องแลกเปลี่ยนชนิดท่อความร้อน

Keywords : Heat Transfer Rate; Transient Condition; Heat Pipe Heat Exchanger

** ผู้นิพนธ์ประสานงานไปรษณีย์อิเล็กทรอนิกส์ supattra.boothaisong@gmail.com โทร. 09 0413 4406*

1. Introduction

A heat pipe is a device with very high thermal conductance. The basic heat pipe consists of a wall, wick, and working fluid. The wick is constructed, for example, from a few layers of fine gauze and fixed to the inside surface of the wall, and capillary forces return the condensate to the evaporator. The analysis of a heat pipe can be divided into the analysis of the heat conduction at the wall, analysis of the fluid flow in the mesh wick, and vapor flow within the vapor core of a heat pipe. From the above analysis, is possible for the heat transfer characteristics of a heat pipe to be estimated as shown in Figure 1. Today, one of the largest applications of heat pipe technology is the cooling of electronic components, such as central processing units (CPUs), circuit boards, and transistors (Payakaruk, Terdtoon *et al.*, 2000). Modeling is often used to predict the performance of heat pipes. Performance analysis, including the concept of temperature distribution, frozen startup behavior of a heat pipe, and an equation for analyzing the temperature distribution of the heat pipe wall (Faghri, 1995), has been part of the modeling process. These analytical models are used for predicting the transient performance of a type of plate heat pipe. Patrix et al. created a mathematical model in MS office Excel Basic to determine the relations of the heat transfer limitations, which defines the boundaries of the heat pipe performance. The limitation values depend on the heat pipe parameters, wick structure parameters, and the thermophysical properties of the working fluid (Nemec, Čaja *et al.*, 2013). The modeling results revealed that the thermal diffusivity, thickness of wall and wick, and heat input pattern affected the heat pipe time constants. The wicks created the main thermal resistance, resulting in the largest temperature drop in the heat pipe (Wang e Vafai, 2000). Tournier produced a model of a heat pipe to predict the transient values of the vapor and wall temperatures as well as the effective power throughput, which were in reasonable agreement with experimental results (Tournier e El-Genk, 1994). The effect of different parameters, such as wall thermal conductivity, wick porosity, and heat pipe dimensions, on heat pipe operation was also considered. A transient model for a micro-grooved heat pipe of any polygonal shape was presented using a macroscopic approach (Suman, De *et al.*, 2005). The coupled equations of heat, mass, and momentum transfer can be solved to obtain the transient as well as steady state profiles of various parameters, namely the substrate temperature, liquid velocity, and liquid pressure, etc. Choudhary (Choudhary, Karki *et al.*, 2004) has shown that wrapping a hydrophilic wick fabric on a cold pipe can

significantly reduce the thermal degradation. The model was based on the volume-averaged equations for unsteady transport of heat, water vapor, and liquid water in a porous medium. The wick model also allowed for the presence of a vapor retarder jacket that can be used to reduce the ingress of water vapor into the insulation. The effect of capillary pressure on the performance of the heat pipe was reported by Thuchayapong (Thuchayapong, Nakano *et al.*, 2012). They successfully produced a numerical simulation of two-dimensional heat transfer and fluid flow in a heat pipe at a steady state using the finite element method. After that, the heat pipe was applied to convey heating or cooling water to a heat exchanger. Thermal numerical values were developed by Eui Guk Jung using the nodal approach, and the junction temperature and thermal resistance of the heat pipe and heat transfer fluid for each row were defined. The recovery heat and effectiveness of the heat exchanger were calculated for various configurations and operating conditions. The simulation results agreed with experimental data for normal operation of the heat pipes (Jung e Boo, 2014). Hagens et al. proposed a model to predict heat transfer and calculate the performance of a heat pipe equipped with a heat exchanger based on correlations from the literature. This model yielded a good agreement between the experiments and predictions. Trends have been interpreted with the aid of various findings reported from single-tube thermosyphons (Hagens, Ganzevles *et al.*, 2007).

In this study, a three-dimensional transient mathematical model was developed by the Galerkin approach and used to predict the heat transfer rate as well as the design of the heat pipe heat exchanger using the effectiveness-NTU method. The heat transfer rate profile was also simulated and compared with experimental data from different working fluids.

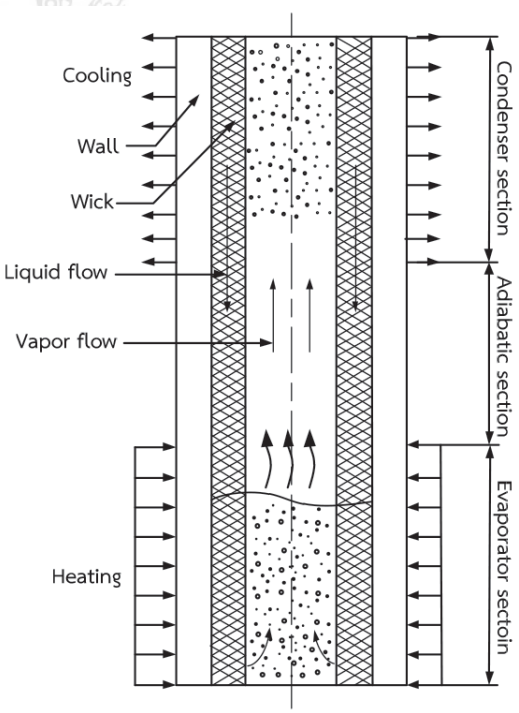

Figure 1 Structure of Conventional Heat Pipe

2. Research Methodology

2.1 Numerical Method

The schematic of the heat pipe and coordinate systems is shown in Figure 2. The components of the heat pipe are the pipe wall, wick structure, and vapor core (vapor of working fluid flow).

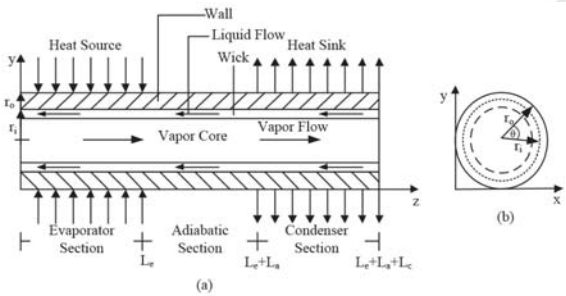

Figure 2 Schematic of Heat Pipe Sections and Coordinate System: along the Length of a Tube (a) and along the Radius of a Tube (b)

The length of the heat pipe was divided into three parts: evaporator section, adiabatic section, and condenser section. Under normal operation, the heat applied to the evaporator section by an external source is conducted through the pipe wall. The three-dimensional transient condition heat conduction equation that describes the temperature in the heat pipe wall is:

$$\rho_w c_{p,w} \frac{\partial T_w}{\partial t} = \frac{k_w}{r}\frac{\partial}{\partial r}\left(r\frac{\partial T_w}{\partial r}\right) + \frac{k_w}{r}\left(\frac{\partial^2 T_w}{\partial \theta^2}\right) + k_w\left(\frac{\partial^2 T_w}{\partial z^2}\right) + \dot{Q}_w \quad (1)$$

where $\rho_w c_{p,w}$ is the effective heat capacity of the pipe wall, k_w is the effective thermal conductivity of the pipe wall which T and t were temperature and time respectively. When heat is applied to the evaporator section, the working fluid in the vapor core is heated and evaporates. Heat is absorbed by vaporizing the working fluid. The vapor travels to the condenser section driven by vapor pressure, were it is cooled and turned back to a saturated liquid. The condensed liquid is returned to the evaporator section using the wick structure that exerts a capillary action on the liquid phase of the working fluid. Therefore, the velocity profile of the liquid phase in the wick structure can be determined using the continuity and momentum equations.

$$\frac{1}{r}\frac{\partial(ru_l)}{\partial r} + \frac{1}{r}\frac{\partial(v_l)}{\partial \theta} + \frac{\partial(w_l)}{\partial z} = 0 \quad (2)$$

$$\rho_l\left(\frac{1}{\varphi}\frac{\partial u_l}{\partial t} + \frac{1}{\varphi^2}\left\{u_l\frac{\partial u_l}{\partial r} + v_l\frac{\partial u_l}{\partial \theta} + w_l\frac{\partial u_l}{\partial z}\right\}\right) = \rho_l g - \frac{\partial p_l}{\partial r} - \frac{\nu_l u_l}{K} + \frac{u_l}{\varphi}\left[\frac{1}{r}\frac{\partial}{\partial r}\left(r\frac{\partial u_l}{\partial r}\right) + \frac{1}{r}\frac{\partial^2 u_l}{\partial \theta^2} - \frac{v_l}{r^2} + \frac{\partial^2 u_l}{\partial z^2}\right] \quad (3)$$

$$\rho_l\left(\frac{1}{\varphi}\frac{\partial v_l}{\partial t} + \frac{1}{\varphi^2}\left\{u_l\frac{\partial v_l}{\partial r} + v_l\frac{\partial v_l}{\partial \theta} + w_l\frac{\partial v_l}{\partial z}\right\}\right) = \rho_l g - \frac{\partial p_l}{\partial \theta} - \frac{\nu_l v_l}{K} + \frac{v_l}{\varphi}\left[\frac{1}{r}\frac{\partial}{\partial r}\left(r\frac{\partial v_l}{\partial r}\right) + \frac{1}{r}\frac{\partial^2 v_l}{\partial \theta^2} - \frac{u_l v_l}{r^2} + \frac{\partial^2 v_l}{\partial z^2}\right] \quad (4)$$

$$\rho_l\left(\frac{1}{\varphi}\frac{\partial w_l}{\partial t}+\frac{1}{\varphi^2}\left\{u_l\frac{\partial w_l}{\partial r}+v_l\frac{\partial w_l}{\partial \theta}+w_l\frac{\partial w_l}{\partial z}\right\}\right)=$$
$$\rho_l g-\frac{\partial p_l}{\partial z}-\frac{\nu_l w_l}{K}+\frac{w_l}{\varphi}\left[\frac{1}{r}\frac{\partial}{\partial r}\left(r\frac{\partial w_l}{\partial r}\right)+\right.$$
$$\left.\frac{\partial^2 w_l}{\partial \theta^2}+\frac{\partial^2 w_l}{\partial z^2}\right] \quad (5)$$

Where ρ is density and u, v, and w are the velocity of the liquid in the wick at r, θ, and the z coordinates, respectively. The continuity equation shown in Eq. (2) explains the law of conservation of mass. The momentum equation consists of the convective term, body force, and pressure term. The last term applied was Darcy's law, which is the friction force in the wick shown in Eqs. (3), (4), and (5). The porosity of the mesh wick as shown in Figure 3 for φ is:

$$\varphi = 1-\frac{\pi AB}{2(1+A)}\sqrt{1+\left(\frac{A}{1+A}\right)^2} \quad (6)$$

where, $A= d/w$, $A= d/s$, and s is the thickness of the wick.

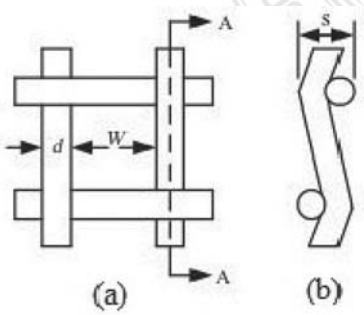

Figure 3 Schematic of Mesh Wick (a) Top View and (b) Cross Section A-A

The energy balance equation explains the law of conservation of energy as shown in Eq. (7). This equation can be used to predict the temperature profile of the liquid phase within the wick structure.

$$(\rho c_p)_{eff}\left(\frac{\partial T_l}{\partial t}+u_l\frac{\partial T_l}{\partial r}+\frac{v_l}{r}\frac{\partial T_l}{\partial \theta}+w_l\frac{\partial T_l}{\partial z}\right)=$$
$$k_{eff}\left[\frac{1}{r}\frac{\partial}{\partial r}\left(r\frac{\partial T_l}{\partial r}\right)+\frac{1}{r^2}\frac{\partial^2 T_l}{\partial \theta^2}+\frac{\partial^2 T_l}{\partial z^2}\right] \quad (7)$$

where, k_{eff} is effective thermal conductivity of the liquid in the wick as:

$$k_{eff}=\frac{k_l\left[(k_l+k_s)-(1-\varphi)(k_l-k_s)\right]}{\left[(k_l+k_s)+(1-\varphi)(k_l-k_s)\right]} \quad (8)$$

where k_l and k_s are the thermal conductivity of the working fluid and material wick, respectively. In the vapor core section, in order to predict the velocity profile of the vapor phase using the continuity equation, the momentum equation, and energy balance equation are shown below:

$$\frac{1}{r}\frac{\partial(r\rho_v u_v)}{\partial r}+\frac{1}{r}\frac{\partial(\rho_v v_v)}{\partial \theta}+\frac{\partial(\rho_v w_v)}{\partial z}+\frac{\partial \rho_v}{\partial t}=0 \quad (9)$$

$$\frac{\partial \rho_v u_v}{\partial t}+u_v\frac{\partial \rho_v u_v}{\partial r}+\frac{v_v}{r}\frac{\partial \rho_v u_v}{\partial \theta}+$$
$$w_v\frac{\partial \rho_v u_v}{\partial z}-\frac{\rho_v v_v^2}{r}=\rho_v g-\frac{\partial p_v}{\partial r} \quad (10)$$

$$\frac{\partial \rho_v v_v}{\partial t}+u_v\frac{\partial \rho_v v_v}{\partial r}+\frac{v_v}{r}\frac{\partial \rho_v v_v}{\partial \theta}+w_v\frac{\partial \rho_v v_v}{\partial z}-$$
$$\frac{\rho_v u_v v_v}{r}=\rho_v g-\frac{\partial p_v}{\partial \theta} \quad (11)$$

$$\frac{\partial \rho_v w_v}{\partial t}+u_v\frac{\partial \rho_v w_v}{\partial r}+\frac{v_v}{r}\frac{\partial \rho_v w_v}{\partial \theta}+w_v\frac{\partial \rho_v w_v}{\partial z}=\rho_v g-\frac{\partial p_v}{\partial z} \quad (12)$$

$$\rho_v c_{p,v}\left(\frac{\partial T_v}{\partial t}+u_v\frac{\partial T_v}{\partial r}+\frac{v_v}{r}\frac{\partial T_v}{\partial \theta}+w_v\frac{\partial T_v}{\partial z}\right)=k_v\left[\frac{1}{r}\frac{\partial}{\partial r}\left(r\frac{\partial T_v}{\partial r}\right)+\frac{1}{r^2}\frac{\partial^2 T_v}{\partial \theta^2}+\frac{\partial^2 T_v}{\partial z^2}\right]+$$

$$2\mu_v\left[\left(\frac{\partial u_v}{\partial r}\right)^2+\left\{\frac{1}{r}\left(\frac{\partial v_v}{\partial \theta}+v_v\right)\right\}^2+\left(\frac{\partial w_v}{\partial z}\right)^2\right]+\mu_v\left[\left(\frac{\partial v_v}{\partial z}+\frac{1}{r}\frac{\partial w_v}{\theta}\right)^2+\left(\frac{\partial w_v}{\partial r}+\frac{\partial u_v}{\partial z}\right)^2+\left(\frac{1}{r}\frac{\partial u_v}{\partial \theta}+r\frac{\partial}{\partial r}\left(\frac{v_v}{r}\right)\right)^2\right]-$$

$$\frac{2}{3}\mu_v\left(\frac{1}{r}\frac{\partial}{\partial r}(ru_v)+\frac{1}{r}\frac{\partial v_v}{\partial \theta}+\frac{\partial w_v}{\partial z}\right)^2+\frac{u_v\partial p_v}{\partial r}+\frac{v_v}{r}\frac{\partial p_v}{\partial \theta}+w_v\frac{\partial p_v}{\partial z} \quad (13)$$

Where μ is the viscosity of vapor.

2.2 Effectiveness-NTU Method

In this paper an analytical model is developed to analyze the performance of the heat pipe heat exchanger based on the effectiveness-NTU method for a sensible heat exchanger. The number of transfer units (NTU) is a dimensionless parameter that is widely used for heat exchanger analysis and has the following values for the evaporator and condenser sections (Noie, 2006):

$$NTU=\frac{UA}{C_{\min}} \quad (14)$$

$$C_h=\dot{m}_h c_{p,h} \quad (15)$$

$$C_c=\dot{m}_c c_{p,c} \quad (16)$$

where U is the overall heat transfer coefficient between $T_{h,i}$ and $T_{c,i}$ encountering the convective heat transfer coefficients h_h and h_c for the two fluids.

$$U=\frac{1}{\frac{1}{h_h}+\frac{1}{h_c}} \quad (17)$$

The maximum possible heat transfer rate ($q_{\max}$) for a heat exchanger can, in principle, be achieved in an infinite length heat exchanger. In such a heat exchanger, the fluid with the lower heat capacity rate of C_h or C_c will experience the maximum possible temperature drop ($T_{h,l} - T_{c,j}$) (Hasan, 2012).

$$q_{\max}=C_{\min}(T_{h,i}-T_{c,i}) \quad (18)$$

The effectiveness of the heat exchanger (ε) is the ratio of the actual heat transfer rate to the maximum possible heat transfer rate.

$$\varepsilon=\frac{q}{q_{\max}} \quad (19)$$

This is dimensionless and must be in the range of $0 \le \varepsilon \le 1$. It is useful because $T_{h,i}$ and $T_{c,i}$ are known. Expressions have

been developed for the effectiveness of a heat exchanger (Frank P. Incropera, 2007; Navarro e Cabezas-Gómez, 2007), as in Eq. (19), and they can take different forms depending on the type of the heat exchanger and the relative flow directions. In this case, a counter flow heat exchanger was used.

$$\varepsilon = \frac{1-\exp\left[-NTU\left(1-C_r\right)\right]}{1-C_r\exp\left[-NTU\left(1-C_r\right)\right]} \quad (20)$$

where C_r is the heat capacity ratio $C_r = C_{\min}/C_{\max}$ wherever $C_r < 1$ and the expressions for other types of heat exchangers can be found in (Kays W. M., 1984).

2.3 Numerical Scheme

The numerical procedure is illustrated in Figure 4. The conservation equations and boundary conditions were solved using the finite element method, while the matrices were derived from these equations using the standard Galerkin approach. The four-node tetrahedron element (Thuchayapong, Nakano *et al.*, 2012) was used as well as the total node number of 221,184. For the calculation procedure of the present simulation program, first, the simulation program generated the grids and assumption that were used for investigating the effect of the temperature on the outer wall of the heat pipe. At both pipe ends, the insulated boundary condition was assumed.

$$\frac{\partial T_{w,v,l}}{\partial r} = 0\,,\ \frac{\partial T_{w,v,l}}{\partial \theta} = 0 \quad (21)$$

At the z coordinate there were three different boundary conditions for the outer wall of the heat pipe. In the evaporator section, constant temperature was supplied during the entire operation. The adiabatic section was insulated and the heat from the condenser section was continuously exchanged by cooling water, as explained in Eq. (22), and the temperature along the pipe wall was calculated by Eq. (1).

$$\begin{cases} T_e = 60^\circ C, 70^\circ C, 80^\circ C & 0 \le z < L_e \\ \dfrac{\partial T_a}{\partial z} = 0 & L_e \le z < L_e + L_a \\ T_c = 20^\circ C & L_e + L_a \le z < L_e + L_a + L_c \end{cases} \quad (22)$$

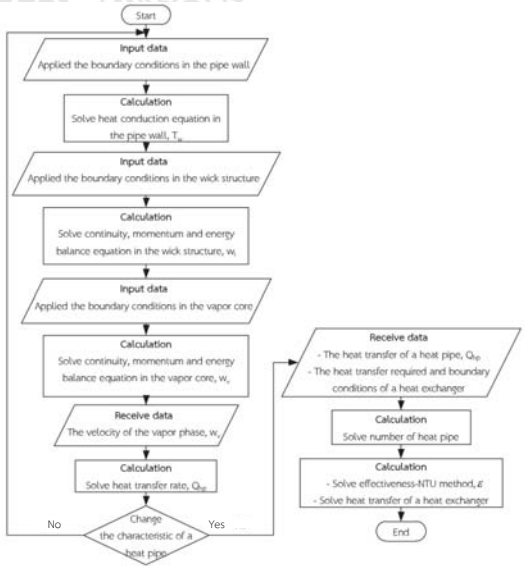

Figure 4 Flow Chart of Numerical Procedure

Next, the velocity and temperature profiles of the liquid phase in the wick structure were calculated from the continuity, momentum, and energy balance equations (Eqs. (2)-(5) and (7)). Thereafter, the velocity and temperature profiles of the vapor phase at the vapor core were calculated using Eqs. (9) and-(13). In the boundary conditions, such values were calculated using Eqs. (23) and (24). At both ends of the pipe, the wick-wall interface and wick-vapor interface showed non-slip movement under the boundary condition, and the liquid velocity was assumed to be zero.

$$u_{v,l} = v_{v,l} = w_{v,l} = 0 \quad (23)$$

The boundary conditions of the velocity of the liquid within the wick and vapor within the vapor core were the three difference boundary conditions used for all z coordinates, so it follows that:

$$\begin{cases} w_{v,l} = \dfrac{\dot{Q}_{in}}{2\rho_{v,l}\pi\, r_{v,l} L_e h_{fg}}, 0 < z \le L_e \\ \dfrac{\partial w}{\partial z} = 0\ ,\ L_e z < L_e + L_a \\ w_{v,l} = \dfrac{\dot{Q}_{out}}{2\rho_{v,l}\pi\, r_{v,l} L_c h_{fg}}, \\ L_e + L_a \le z < L_e + L_a + L_c \end{cases} \quad (24)$$

where, L is length of heat pipe, $\dot{Q}_{in}$ and $\dot{Q}_{out}$ are the total heat input and total heat output at the wall-wick interface in the evaporator section respectively. Use the velocity of the vapor phase to calculate the heat transfer rate of the heat pipe $\dot{Q}_{hp} = w_v 2\rho_v \pi r_v L_c h_{fg}$ Thereafter, use the value of the heat transfer rate of a heat pipe, $\dot{Q}_{hp}$, to determine the heat transfer required $\dot{Q}_{re}$ = 1,000 watt.

2.4 Experimental Method

The experimental apparatus used is shown in Figure 6. The test section consisted of three sections: the evaporator and condenser sections were heated and cooled using water jackets (14x14x15 cm^3) and the adiabatic section was covered with Styrofoam to prevent heat loss to the surroundings. The heating and cooling water entered the water jackets at 60 ^oC, 70 ^oC, or 80 ^oC and 20 ^oC, respectively. The physical dimensions of the heat pipe were inner wall radius (r_i) = 4 mm, outer wall radius (r_o) = 5 mm, L_e = 110 mm, L_a = 20 mm, and L_c = 110 mm. The wick was a one-layered type with a 100 mesh copper solder wick. The mass flow rate was 0.05 kg/s. The outer side of the water jackets in the evaporator and condenser sections was covered with Aeroflex insulation, and the heat pipe was placed vertically in a test position. Seventeen thermocouples were installed for data collection (Yokogawa DX200 with $\pm$0.1°C accuracy, 20 channel input, and -200°C to 1,100°C measurement temperature-range). Type K thermocouples

(OMEGA with $\pm$0.1°*C* accuracy) were used to monitor the temperatures at specified times. The temperature measure points were as follows: four points in the evaporator section, four points in the condenser section, four points in the adiabatic section, a point in each of the inlet and outlet of the evaporator section, a point in each of the inlet and outlet of the condenser section, and a point in the ambient temperature. The heat transfer rate was determined from the experiment using the equation $Q = \dot{m}c_p(T_{out} - T_{in})$. The experimental set-up was as shown in Figure 5 and a photograph of the heat exchanger heat pipe is shown in Figure 6.

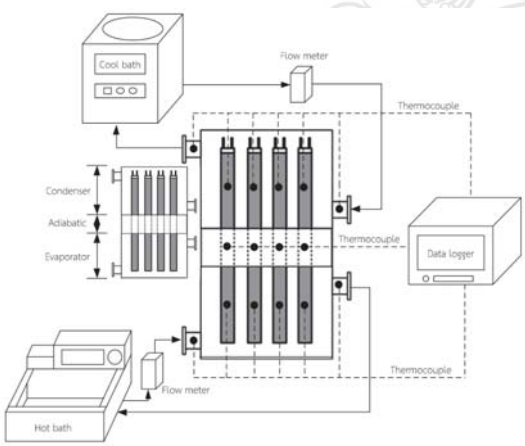

Figure 5 Experimental Setup of Heat Exchanger

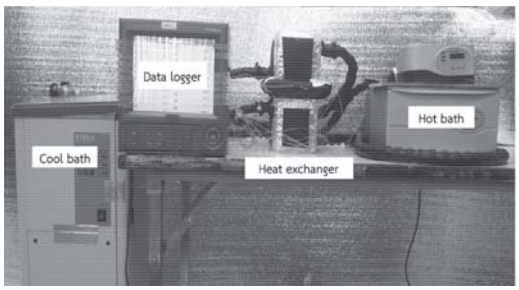

Figure 6 Photograph of Experimental Setup

3. Results and Discussion

According to Eq. (1), the computation domain in the radial (r), angle (θ) and axial (z) coordinates of the three-dimensional model is represented in Figure 7 and the temperature in the evaporator section was 60°*C*. The working fluid was R134a. The water-cooling at the condenser section was 20°*C*. We describe the results of the experimental model by comparing them to the three-dimensional model. The transient temperature profiles were average values at the evaporator section, adiabatic section, and condenser section, and were plotted as functions of time. The lines correspond to the experimental average values of the temperatures at each section, and the three-dimensional model predicted the response of the temperature with time. The times required to reach the steady state were about 1,160 seconds and 1,200 seconds for the simulation and experimental results respectively. As can be seen from the figures, the comparisons of the response curves between the results of the experimental

method and three-dimensional model are excellent for all three sections.

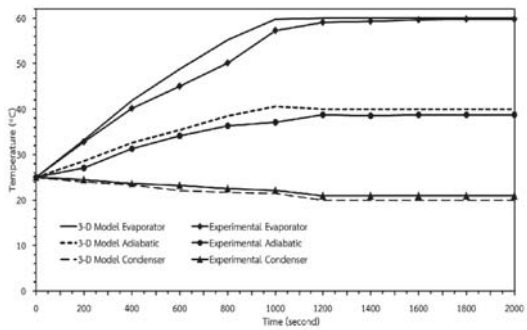

Figure 7 Outer Wall Temperature Profiles with Time

The transient temperature profiles in the condenser section rose during start-up from the initial temperature to the input outer wall temperature. The adiabatic section was not affected by the ambient heat, but was induced by thermal conduction from the evaporator section, and thus the temperature of the adiabatic section increased until it reached a steady state. However, the transient temperature profiles in the condenser section decreased because the temperature at the outer wall was less than the initial temperature of the condenser section.

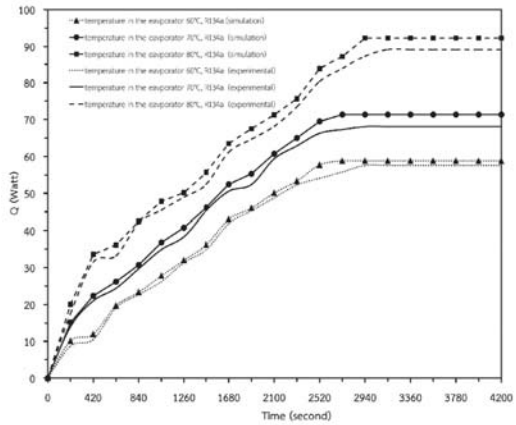

Figure 8 Heat Transfer Rate Profile of Heat Pipe

The heat transfer rate profile for the transient condition to the steady state of a heat pipe simulation in comparison with experimental results are shown in Figure 8. The triangle symbol and dotted line represent the heat transfer rate profiles of a heat input at the evaporator section of 60°C, and it can be seen that the time to reach the steady state was 2,560 second. The circle symbol and solid line represent the heat transfer rate profiles of a heat input at the evaporator section of 70°C, and it can be seen that the time to reach the steady state was 2,700 second. The square symbol and dashed line represent the heat transfer rate profiles of a heat input at the evaporator section of 80°C, and it can be seen that the time to reach the steady state was 2,940 second. Since the time to reach a steady state depended on the heat input at the evaporator section, when the heat input at the evaporator section increased, the time to reach a steady state

increased. As can be seen from the heat transfer rate profiles of the simulation and experimental results, they are very close with differences of 2.0%, 4.6%, and 3.3% for the heat inputs at the evaporator section of 60°C, 70°C and 80°C, respectively.

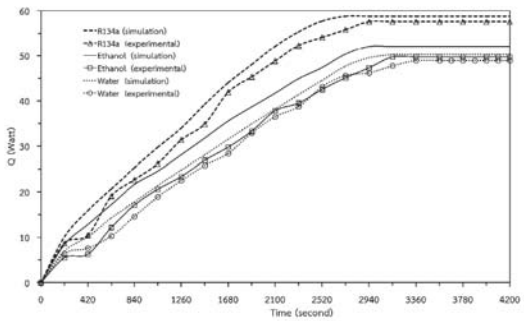

Figure 9 Comparisons of Working Fluid Heat Transfer Rate Profiles

Figure 9 shows the comparisons of the simulation model and experimental method heat transfer rate profiles under the transient condition of the heat pipe. These figures show the time required to reach a steady state as 3,045 seconds for the simulation model and 3,360 seconds for the experimental data when the working fluid was distilled water. The times using ethanol for the simulation and experimental methods were 2,940 seconds and 3,100 seconds, respectively. While it was seen that the times required to reach a steady state were 2,520 seconds and 2,900 seconds for the simulation and experimental methods using R134a. Therefore, the time required to reach a steady state depended on the working fluid used. It can be seen that the heat transfer rate profiles between the simulation and experimental methods were very similar, with differences of 3.3%, 4.6%, and 2.0% for the working fluids of distilled water, ethanol, and R134a, respectively.

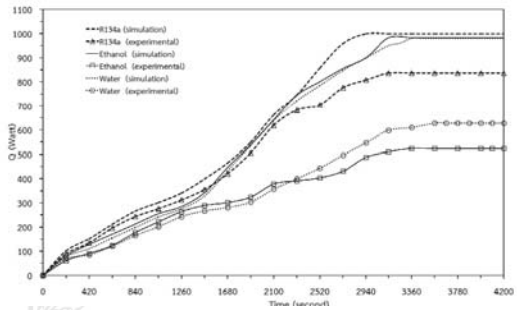

Figure 10 Heat Transfer Rate Profiles from Heat Pipe Heat Exchanger

The comparison of the simulation model and experimental method heat transfer rate profiles under the transient condition of the heat pipe heat exchanger show that the time required to reach a steady state was 3,200 seconds for the simulated model and 3,570 seconds from experimental method when the working fluid was distilled water. The times when ethanol was used were for simulation and experiment methods were 3,010 seconds and 3,360 seconds, respectively. It was seen that the times required to reach a steady state were 2,940 seconds and 3,150 seconds for the simulation and experimental methods when using R134a, as shown in Figure

10. It can be seen that the heat transfer rate profiles between the simulation and experimental methods were very similar, with the differences being 10.3%, 10.4%, and 6.7% for the working fluids of distilled water, ethanol, and R134a, respectively. As can be seen from these figures, the heat transfer rate was 627.3 watts when the working fluid was distilled water. The heat transfer rate using ethanol for the heat exchanger heat pipe was 522.8 watts. While it can be seen that the heat transfer rate was 836.4 watts using R134a. It was found that the heat transfer rate of the heat exchanger heat pipe depended on the working fluid: if the working fluid had a high thermal conductivity then there will be a high heat transfer rate.

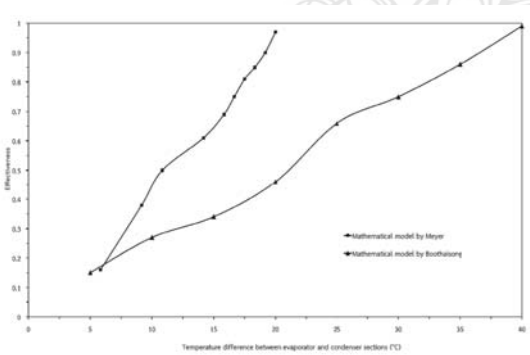

Figure 11 Effectiveness of Heat Pipe Heat Exchanger

Now, we will describe the effectiveness of the heat exchanger when compared with analytical data obtained by Meyer *et al*., as shown in Figure 11. Their model was a heat pipe heat exchanger for a mini-drier (Meyer and Dobson, 2006). While, the present study involved a three-dimensional model in the transient condition of a cylindrical heat pipe wall, so it has to become normalized by the temperature difference between the evaporator and condenser sections. It appears that the trend is one of similar effectiveness. The effectiveness increased when the temperature difference between the evaporator and condenser sections increased.

4. Conclusions

Transient three-dimensional simulations of the heat exchanger heat pipe have been successfully simulated using the finite element method. The temperatures from the developed three-dimensional model of the outer wall were in good agreement with the experimental data. A heat input on the evaporator of 60°C had the shortest time required to reach a steady state. The calculation time was about 2,560 second using a desktop computer with a CPU operating frequency of 3.90 GHz.

The benefit of this work is a three-dimensional simulation that gives calculated values that are correct and accurate. The weakness of this study is that it needed a lot of the time for the simulation modeling. The present simulation codes are still under development for the overall heat pipe

simulation, and they should become a strong tool to predict the overall heat pipe operation in the future.

5. Acknowledgments

The authors gratefully acknowledge the Royal Golden Jubilee Ph.D. Program (Grant No. PHD/0014/2554) under the Thailand Research Fund (TRF) for funding this research.

6. References

Payakaruk T., P. Terdtoon and S. Rittidech, 2000. Correlations to predict heat transfer characteristics of an inclined closed two-phase thermosyphon at normal operating conditions. **Applied Thermal Engineering**, 20 (9): 781-790.

Faghri, A. 1955. Heat Pipe Science And Technology. **Washington DC: Global Digital Press**.

Nemec, P., A. Čaja and M. MALCHO, 2013. Mathematical model for heat transfer limitations of heat pipe. **Mathematical and Computer Modelling**, 57(1-2): 126-136.

Wang, Y., and K. Vafai, 2000. Transient characterization of flat plate heat pipes during startup and shutdown operations. **International Journal of Heat and Mass Transfer**, 43(15): 2641-2655.

Tournier, J.M., and M.S. El-Genk, 1944. A heat pipe transient analysis model. **International Journal of Heat and Mass Transfer**, 37(5): 753-762.

Suman, B., S. De and S. Dasgupta, 2005. Transient modeling of micro-grooved heat pipe. **International Journal of Heat and Mass Transfer**, 48(8): 1633-1646.

Choudhary, M.K., K.C. Karki and S.V. Patankar, 2004. Mathematical modeling of heat transfer, condensation, and capillary flow in porous insulation on a cold pipe. **International Journal of Heat and Mass Transfer**, 47(26): 5629-5638.

Thuchayapong, N., et al. 2012. Effect of capillary pressure on performance of a heat pipe: Numerical approach with FEM. **Applied Thermal Engineering**, 32: 93-99.

Jung, E.G., and J.H. BOO, 2014. Thermal numerical model of a high temperature heat pipe heat exchanger under radiation. **Applied Energy**, 135: 586-596.

Hagens, H., et al. 2007. Air heat exchangers with long heat pipes: Experiments and predictions. **Applied Thermal Engineering**, 27(14-15): 2426-2434.

Noie, S.H. 2006. Investigation of thermal performance of an air-to-air thermosyphon heat exchanger

using ε-NTU method. **Applied Thermal Engineering**, 26(5–6): 559-567.

Hasan, A. 2012. Going below the wet-bulb temperature by indirect evaporative cooling: Analysis using a modified ε-NTU method. **Applied Energy**, 89(1): 237-245.

Navarro, H.A., and L.C. Cabezas-Gómez, 2007. Effectiveness-ntu computation with a mathematical model for cross-flow heat exchangers. **Brazilian Journal of Chemical Engineering**, 24: 509-521.

Frank, D.P.D., P. Incropera, B.L. Theodore and L.S. Adrienne, 2007. Fundamentals of heat and mass transfer. **Hoboken: John Wiley & Sons (Asia) Pte. Ltd.**

KAYS W.M., and A.L. London, 1984. Compact heat exchangers. **New York: McGraw-Hill**.

Meyer, A., and T.R. Dobson, 2006. A heat pipe heat recovery heat exchanger for a mini-drier. **Journal of Energy in Southern Africa**, 17(1): 50-57.